Biomech Model Mechanobiol (2011) 10:27–38
DOI 10.1007/s10237-010-0216-8

ORIGINAL PAPER

Mechanical characterisation of in vivo human skin using a 3D force-sensitive micro-robot and finite element analysis

Cormac Flynn · Andrew Taberner · Poul Nielsen

Received: 28 October 2009 / Accepted: 8 April 2010 / Published online: 29 April 2010

Abstract The complex mechanical properties of skin have been the subject of much study in recent years. Several experimental methods developed to measure the mechanical properties of skin in vivo, such as suction or torsion, are unable to measure skin's anisotropic characteristics. An experiment characterising the mechanical properties of in vivo human skin using a novel force-sensitive micro-robot is presented. The micro-robot applied in-plane deformations to the anterior forearm and the posterior upper arm. The behaviour of the skin in each area is highly nonlinear, anisotropic, and viscoelastic. The response of the upper arm skin is very dependent on the orientation of the arm. A finite element model consisting of an Ogden strain energy function and quasi-linear viscoelasticity was developed to simulate the experiments. An orthogonal initial stress field, representing the in vivo skin tension, was used as an additional model parameter. The model simulated the experiments accurately with an error-of-fit of 17.5% for the anterior lower forearm area, 6.5% for the anterior upper forearm and 9.3% for the posterior upper arm. The maximum in vivo tension in each area determined by the model was 6.2 Nm^{-1} in the anterior lower forearm, 11.4 Nm^{-1} in anterior upper forearm and 5.6 Nm^{-1} in the posterior upper arm. The results also show that a finite element model with a neo-Hookean strain energy function cannot simulate the experiments with the same accuracy.

Keywords Human skin · Anisotropy · Viscoelasticity · In vivo tension · Constitutive modelling

C. Flynn (✉) · A. Taberner · P. Nielsen
University of Auckland, Auckland Bioengineering Institute,
70 Symonds Street, Auckland, New Zealand
e-mail: c.flynn@auckland.ac.nz
URL: http://www.abi.auckland.ac.nz/

List of symbols

F_A, F_B, F_C	Forces measured at each force transducer
R_X, R_Y, R_Z	Reaction force components at probe tip
w	Distance from centroid to apex of triangle formed by the transducers
h	Perpendicular distance between probe tip and base of rigid frame
W	Strain energy
μ, α	Ogden function material parameters
$\lambda_1, \lambda_2, \lambda_3$	Principal stretches
p	Lagrange multiplier representing hydrostatic pressure
J	Volume ratio
C_{10}	Neo-Hookean function material parameter
T_e	Elastic stress component
g_R	Reduced relaxation function
$\bar{g}_1^{\mathrm{P}}, \tau_1^{\mathrm{G}}$	Prony series parameters
σ_X, σ_Y	Initial pre-stress in X and Y directions
R_i^{model}	Reaction force at probe tip calculated from model
$R_i^{\exp}$	Reaction force at probe tip measured in experiment

1 Introduction

Human skin is a complex material, which exhibits nonlinear stress-strain, anisotropic, and viscoelastic characteristics (Daly 1982; Schneider 1982; Silver et al. 2001; Har-Shai et al. 1996; Kvistedal and Nielsen 2009). In addition, skin in vivo is in tension, which varies according to location, age, and person (Alexander and Cook 1977). The measurement of the mechanical properties of skin in vivo is important in many diverse areas: the mechanical properties are an

indicator of the state of health of the tissue (Wilkes et al. 1973); Accurate knowledge of the mechanical properties of skin would allow for the improved design of artificial skin (Bellamy et al. 2003); An accurate model of in vivo skin would be useful in developing strategies to improve the healing of acute or chronic wounds (Cacou and Muir 1995) and designing surgical incision patterns to minimise scarring (Lott-Crumpler and Chaudhry 2001).

Several experimental methods have been developed to measure the mechanical properties of skin in vivo. These methods include applying uniaxial or biaxial tension (Wan Abas 1994), suction (Delalleau et al. 2008; Diridollou et al. 2000; Hendriks et al. 2006; Khatyr et al. 2006), torsion (Batisse et al. 2002), and normal indentation (Pailler-Mattei et al. 2008; Delalleau et al. 2006) to the skin under study. Some of these methods, such as biaxial tension, apply in-plane deformations in only one or two directions. Suction, torsion, and normal indentation tests are unable to measure the skin's anisotropy due to the axisymmetric nature of the tests. In order to characterise the complex mechanical properties of skin, it is necessary to apply a rich set of deformations to the region of interest.

Various constitutive models have been used to simulate in vivo experiments of skin. Many of these models assume skin to be an isotropic, linear elastic material (Zahouani et al. 2009; Diridollou et al. 2000; Pailler-Mattei et al. 2008; Khatyr et al. 2006). In these cases, the skin is often characterised by a Young's modulus and Poisson's ratio. Delalleau et al. 2008) used two Young's moduli to characterise skin in suction tests—one represented the stiffness of skin at low strains and the other represented the stiffness of skin at higher strains. Representing a highly nonlinear material such as skin using a Young's modulus in a linear or quasi-linear model is a very simplified approach. Hendriks et al. (2006) used an extended Mooney–Rivlin strain energy function to model the response of skin in suction tests. While the model simulated the nonlinear response of skin with reasonable accuracy, they assumed skin to be an isotropic elastic material. This model, as well as many others in the literature, ignores the tension inherent in living skin. The in vivo tension has been shown to be an important parameter when modelling the behaviour of skin around scars and sutured wounds (Cerda 2005; Flynn and McCormack 2008b; Cavicchi et al. 2009). Evans (2009) recently used an Ogden strain energy function with a pre-strain parameter to simulate in-plane deformations of forearm skin. The initial strain parameter represented the in vivo tension. However, the model ignored the anisotropy present in skin. Bischoff et al. (2000) simulated in vivo extensometer test data from Gunner et al. (1979) using an Arruda–Boyce strain energy function with an anisotropic pre-stress. They also demonstrated the ability to model anisotropic in vitro test data using an isotropic strain energy function with an anisotropic stress distribution.

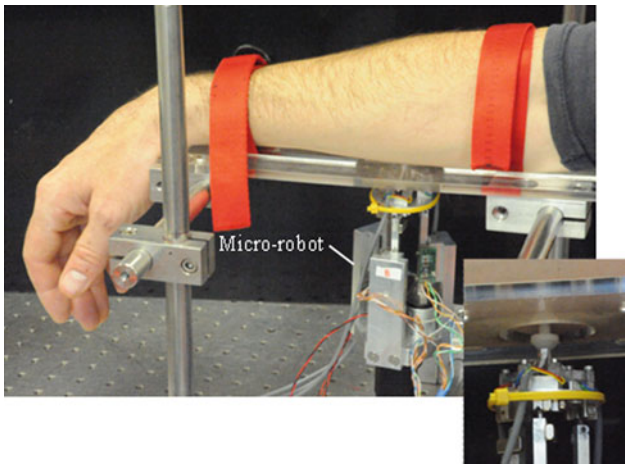

Fig. 1 Experimental set-up. Inset figure shows the probe attached to the skin of the anterior upper forearm

All the models mentioned so far have also ignored the viscoelastic properties of skin. Viscoelasticity can be modelled using a state-variable approach where history dependent variables are determined using evolution equations for their time-rates of change (Rubin et al. 1998; Bergstrom and Boyce 2001). The quasi-linear viscoelasticity approach of Fung (1993) has been widely used to model viscoelasticity in a variety of soft tissues including skin. It has modelled the hysteresis observed in biaxial tests of in vitro human skin (Shoemaker et al. 1986) and simulated accurately stress relaxation tests of porcine skin (Bischoff 2006). This approach can simulate viscoelastic effects with a minimum number of parameters.

This paper details the characterisation of the mechanical properties of the skin of different areas of the arm using in vivo experiments and finite element analyses. The experimental apparatus and procedure are first outlined, followed by a description of the finite element models and nonlinear optimisation procedures. The paper demonstrates the ability of an Ogden strain energy function with viscoelasticity and an anisotropic pre-stress to accurately capture the behaviour of the skin of the arm.

2 Materials and methods

2.1 Laboratory experiment

The experimental set-up consists of a novel force-sensitive micro-robot that applied controlled deformations to the skin, and a support plate upon which to rest the arm under study (Fig. 1).

The micro-robot has three parallel axes, each driven by a voice-coil actuator (BEI KIMCO LA10-12-027A), a moving platform, three force transducers (FSS1500NC,

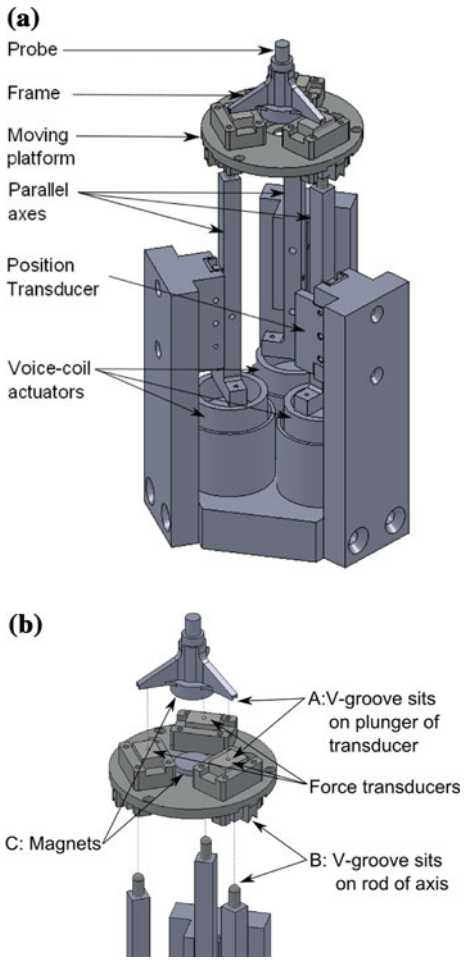

Fig. 2 **a** Force-sensitive micro-robot. **b** Exploded view of top section of micro-robot

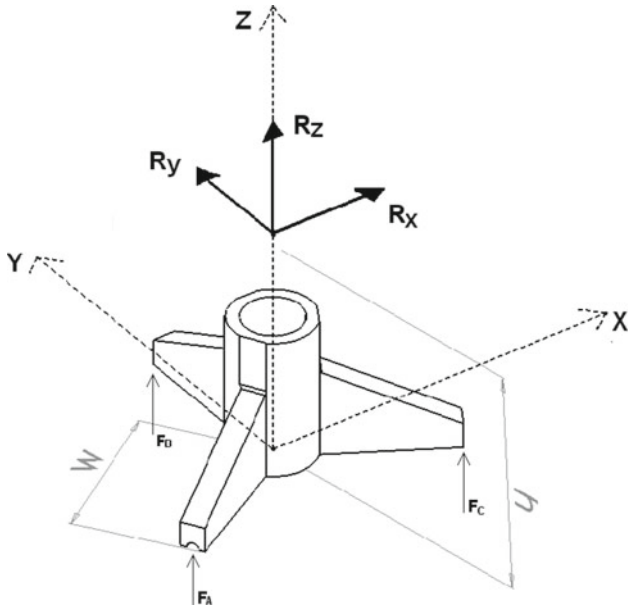

Fig. 3 Calculating the reaction force vector at the probe tip (R_X, R_Y, R_Z) from the forces measured from the force transducers, F_A, F_B, F_C

Honeywell, Freeport Illinois, USA), three linear position transducers (RDC1014, ALPS, Campbell California, USA), a rigid frame, and a probe (Fig. 2). Each axis is guided by a precision linear slide (IKO BSP 730SL). On top of each axis, there is a short rod with a hemispherical end. Underneath the moving platform are three v-grooves, each of which sits on top of the rod of an axis (Label B on Fig. 2(b)). A magnet on each axis and v-groove keeps the moving platform connected to the axes. The position transducers measure the displacement of each actuator. They had a repeatability of 63 μm and a sensitivity of about 0.5 V/mm. The linearity of the devices was within ±0.5%. The linear transducers were calibrated by displacing each axis in steps of 50 μm using a micrometer gauge with a resolution of 10 μm. The voltage output was measured for each step and a linear equation relating voltage to displacement was found. The force transducers had a repeatability of 0.1 N and a sensitivity of 0.12 mV/g. The linearity of the transducers was ±1.5%. They were calibrated by placing weights ranging from 0.1 to 14 N on them. The voltage output for each applied weight was recorded and a linear equation relating the output voltage to the applied force was found.

The force transducers are fixed to the moving platform, each at the apex of a 15-mm equilateral triangle. A v-groove underneath each leg of the rigid frame sits on the plunger of the force transducer (Label A on Fig. 2b). Two magnets, positioned on the bottom of the rigid frame and the top of the moving board, keep the rigid frame in place (Label C on Fig. 2b). A 4-mm-diameter cylindrical probe is attached to the tip of the rigid frame. Knowing the force measured by each force transducer enables the force vector applied at the probe tip to be calculated using a straightforward static analysis of the frame in Fig. 3:

$$\begin{bmatrix} R_X \\ R_Y \\ R_Z \end{bmatrix} = \begin{pmatrix} -\sqrt{3}w/2h & 0 & \sqrt{3}\,w/2h \\ -w/2h & w/h & -w/2h \\ -1 & -1 & -1 \end{pmatrix} \begin{bmatrix} F_A \\ F_B \\ F_C \end{bmatrix} \quad (1)$$

where R_X, R_Y, R_Z are the X, Y, and Z components of the reaction force at the probe tip, respectively, F_A, F_B, F_C are forces measured at each force transducer, w is the distance from the centroid to an apex of the triangle formed by the three force transducers, and h is the perpendicular distance between the probe tip and the base of the rigid frame (Fig. 3).

The displacement of the probe tip was calculated from the displacement of the three axes using a forward kinematics algorithm. The details of the algorithm are in the appendices.

A LabView software interface (National Instruments, Austin, USA) allowed the user to control the motion of the actuators and store the acquired data. A signal is sent from the

motion control card (NI 7358, National Instruments, Austin, USA) and amplified to drive the voice-coil actuators. The signals from the position and force transducers are read by the data acquisition cards (NI PCI-6221, National Instruments, Austin, USA). The position signals of the actuators are also fed back to the motion control card giving closed-loop control. The resolution of the probe displacement was 50 μm, and the resolution of the force measured at the probe tip was 30 mN.

The support plate was positioned above the micro-robot. Two restraining straps were used to prevent unwanted movement of the arm. A 40-mm-diameter hole was located in the centre of the support plate. The area of skin under study was above this hole. Double-sided tape was placed around the edge of the hole so that the skin in contact with the edge of the hole did not move. The inside edge of the tape matched the edge of the 40-mm-diameter hole.

The tests were performed on three areas of the right arm—the posterior upper arm, the upper anterior forearm, and the lower anterior forearm (Fig. 4a). The arm of the volunteer was rested on a support with the area of interest facing downwards. The cylindrical probe was attached to the surface of the skin using liquid cyanoacrylate adhesive. The adhesive was uniformly placed on the probe surface only. The actuators moved the probe such that the surface of the skin was subject to an in-plane cyclical deformation with a peak-to-peak amplitude of about 1.5 mm and a frequency of 0.1 Hz. Three cycles were performed to pre-condition the skin. The time, displacement, and the reaction force at the probe tip were recorded for each cycle. The deformation was repeated in directions 0, 30, 60, 90, 120, and 150° relative to the longitudinal axis of the arm (Fig. 4b). The experiments were repeated three times.

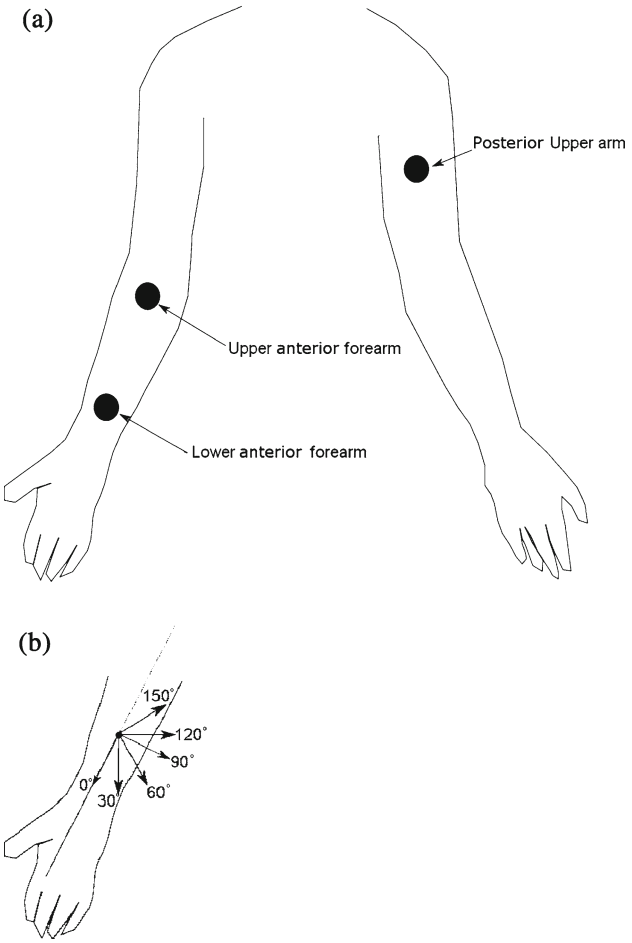

Fig. 4 **a** The three areas of the *right arm* that were studied—anterior *lower forearm*, anterior *upper forearm* and posterior *upper arm*. **b** At each site, the probe was displaced in five different directions relative to the longitudinal axis of the arm

3 Finite element model

3.1 Geometry and boundary conditions

A finite element model of the experiment was created using ABAQUS/Standard Version 6.7.1 (SIMULIA, Providence, RI) (Fig. 5a). A circular skin area of diameter 40 mm was modelled. This represented the skin located within the hole on the support plate. When the probe displacement was 0 and 90° relative to the longitudinal axis of the arm, the problem was assumed to be symmetrical and so only half the domain was modelled (Fig. 5b). In those two cases, symmetrical boundary conditions were placed along the appropriate sides. The edge of the domain was restricted from moving in all degrees of freedom. A 4-mm-diameter area in the centre of the domain (referred to as the probe contact area) was partitioned to represent the area of contact between the probe and the skin. The domain was meshed using linear quadrilateral and trilateral shell elements. The thickness of the shell elements were 1.5 mm representing the average thickness of the skin on the arm (Reihsner et al. 1995). The full models contained 2,012 elements and 2,039 nodes, while the symmetrical models contained 1,016 elements and 1,064 nodes. The mesh density was doubled until there was convergence in the reaction forces of the nodes in the probe area of the model.

3.2 Constitutive model

An Ogden strain energy function was used as the constitutive model of skin

$$W = \frac{2\mu}{\alpha^2}\left(\lambda_1^{\alpha} + \lambda_2^{\alpha} + \lambda_3^{\alpha}\right) - p\,(J-1) \tag{2}$$

where μ and α are material parameters; $\lambda_1, \lambda_2, \lambda_3$ are the principal stretches; p is a Lagrange multiplier representing

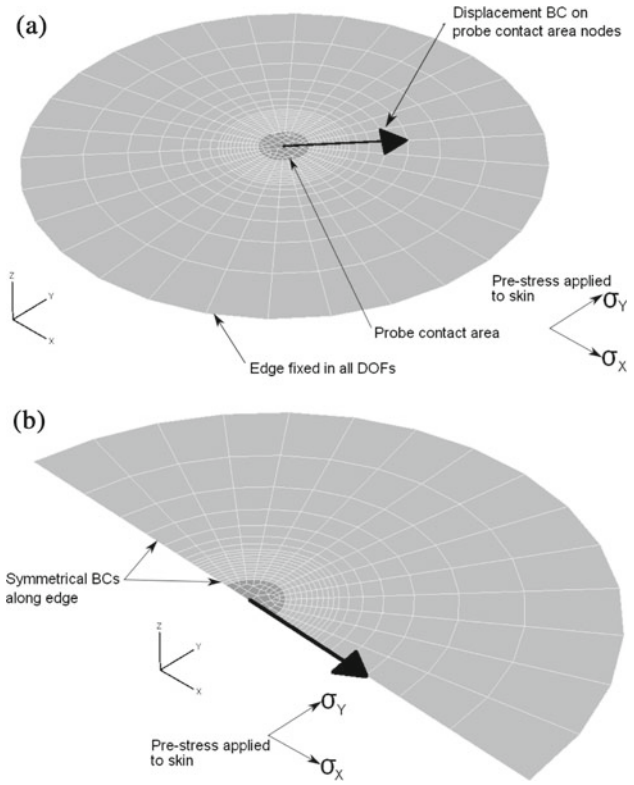

Fig. 5 Finite element models of experiment. When the probe displacement is in a direction 30 and 60° relative to the longitudinal axis of the arm, a full model is used (**a**); for 0 and 90° directions a symmetrical model suffices (**b**). The edge of the domain is fixed in all degrees of freedom representing the contact between skin and the double-sided tape on the edge of the hole of the support plate. An initial pre-stress is applied in the *X* and *Y* directions. The nodes in the *shaded* section in the centre of the domain representing the probe contact area are displaced in the *X*-*Y* plane

hydrostatic pressure; and J is the volume ratio, which is given by the determinant of the deformation gradient.

For comparison purposes, a neo-Hookean strain energy function was also used in the constitutive model of skin for some of the simulations

$$W = C_{10}\left(\lambda_1^2 + \lambda_2^2 + \lambda_3^2\right) - p\,(J-1) \tag{3}$$

where C_{10} is a material parameter.

The total stress in the specimen is assumed to be equal to an elastic stress, $T_e\,[\lambda\,(t)] = \lambda \partial W/\partial\lambda$, due to the instantaneous tissue response decreased by a viscous component depending on the past history. From Fung (1993), the stress at time t is given by

$$T(t) = T_e\,[\lambda\,(t)] + \int_0^t T_e\,[\lambda\,(t-\tau)]\,\frac{\partial g_R\,(\tau)}{\partial \tau} d\tau \tag{4}$$

where $g_R(t)$ is the reduced relaxation function, which characterises the material's viscoelastic response. $g_R\ (t)$ is represented by a Prony series as follows:

$$g_R(t) = 1 - \bar{g}_1^{\mathrm{P}}\left(1 - e^{-t/\tau_1^{\mathrm{G}}}\right) \tag{5}$$

where $\bar{g}_1^{\mathrm{P}}$ and τ_1^{G} are material parameters.

4 Analysis procedure

The finite element models were solved using an implicit quasi-static algorithm available in ABAQUS/Standard through the *VISCO keyword. A suggested initial time increment of 0.02 s was specified. The maximum time step allowed was 0.2 s. The default convergence criteria in ABAQUS/Standard were used.

An initial stress was applied to the domain in the X and Y directions representing the in vivo tension inherent in living skin. This pre-stress was applied to the model using the *INITIAL CONDITIONS, TYPE=STRESS facility in ABAQUS. A stress field is imposed on each element in the model in its initial reference state. The amount of pre-stress was determined through the nonlinear optimisation procedure, which is described in the next section. The displacement of the probe was simulated by applying appropriate displacement boundary conditions to the nodes within the probe contact area. The displacement and speed of the probe in the finite element analysis were the same as the displacement and speed of the probe in the corresponding experiment. The reaction force of the probe in the model was found by summing the reaction forces of all the nodes within the probe area of the finite element mesh.

4.1 Nonlinear optimisation

For each location of the arm, there were six model parameters to determine—the four material parameters μ, α, $\bar{g}_1^{\mathrm{P}}$, τ_1^{G}, and the initial stress in the X and Y directions σ_X and σ_Y. The parameter values that best fit the model to the pre-conditioned experimental data were found using the nonlinear optimisation techniques. The *lsqnonlin* function in MATLAB Version 7.5 (The MathWorks, Inc., Natick, MA, USA), which uses a trust-region method, was used to minimise the following objective function in a least-squares sense

$$F_i(\mathbf{x}) = \sum_{i=1}^{n}\left(R_i^{\mathrm{model}}(\mathbf{x}) - R_i^{\mathrm{exp}}\right)^2 \tag{6}$$

where n is the number of data points (about 330 for this study), $\mathbf{x}$ is a vector representing the model parameters, $R_i^{\mathrm{model}}(\mathbf{x})$ is the probe reaction force calculated from the model, and R_i^{exp} is the measured experimental probe reaction force at the ith datapoint.

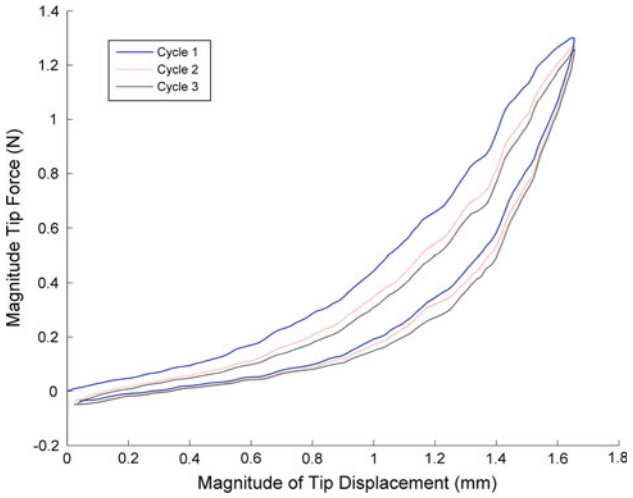

Fig. 6 Three force–displacement cycles for the *upper arm*. The probe was displaced in a direction 90° to the longitudinal axis of the *right arm*

5 Results

A typical probe-tip force–displacement curve from the experiments is shown in Fig. 6. For all skin areas tested, the response was highly nonlinear and contained significant hysteresis. Also, the difference between the first and second loading cycle was much greater than the difference between the second and third loading cycle. This indicated that the skin was almost pre-conditioned after the first cycle.

The force–displacement response on the posterior upper arm was anisotropic (Fig. 7a). The response was stiffest when the probe was displaced in a direction 90° to the longitudinal axis of the arm and least stiff when the probe was displaced along the longitudinal axis of the arm. When the arm was bent 90°, the response was more isotropic than when the arm was straight (Fig. 7b). The force response was slightly stiffer when the probe displacement was along the longitudinal axis of the arm. There was less anisotropy in the force–displacement curves for the anterior upper forearm (Fig. 7c). The responses for all the directions were similar with a peak probe-tip force of 1.6 N at a displacement of about 1.5 mm. Only the 0 and 90° directions are shown for clarity. For the anterior lower forearm, the response in the 90° direction was stiffest, while the response in the 0° direction was the least stiff (Fig. 7d).

For the posterior upper arm and the anterior lower forearm, the reaction force at 1.4- mm probe displacement was a maximum when the angle of displacement was 90° (Fig. 8). For angles of displacement greater or less than 90°, the reaction force at 1.4 mm decreased monotonically. For the anterior upper forearm, the reaction force at 1.4 mm probe displacement was a maximum when the displacement angle was 150°. For displacement angles greater or less than 150°, the reaction force decreased monotonically.

Comparing the overall response of the different skin areas, the anterior upper forearm was the stiffest, followed by the posterior upper arm (Fig. 9). The skin of the anterior lower forearm was the least stiff of the three areas. For tip displacements up to 0.5 mm, the tangent stiffness of the anterior upper forearm was about 0.6 Nmm^{-1}; the tangent stiffness of the upper arm was 0.2 Nmm^{-1}; and the stiffness of the lower anterior forearm was 0.1 Nmm^{-1}. For tip displacements from 1.2 to 1.5 mm, the tangent stiffness of the anterior upper forearm and upper arm was about 1.8 Nmm^{-1} and the tangent stiffness of the anterior upper forearm was 1.2 Nmm^{-1}.

Model parameters were found using nonlinear optimisation that best fit the finite element analyses to the experiments. The results of the simulations are shown along with the experimental results in Figs. 7a–d, while the model parameters for each skin area are listed in Table 1. The pre-strain that is equivalent to the calculated pre-stress is also listed. The error-of-fit of the model to the experiment was calculated for each case. The error-of-fit is defined as

$$\mathrm{Error-of-fit} = \frac{\sum_{i=1}^{N} \left| R_i^{\mathrm{model}} - R_i^{\mathrm{exp}} \right|}{\sum_{i}^{N} \left| R_i^{\mathrm{exp}} \right|} \times 100\% \qquad (7)$$

There was a good match between all the experimental and finite element results with error-of-fits ranging from 6.5% for the anterior upper forearm to 17% for the anterior lower forearm. For the posterior upper arm, the material parameters determined when the arm was straight were also used for the case when the arm was bent. Only the pre-stress was varied in the nonlinear optimisation. A good fit was found with an error of 7.2% between the experimental and model results for the bent arm by changing only the pre-stress in the skin. The reaction forces predicted by the models at 1.4 mm probe displacement for different angles of displacement are compared with the experimental results in Fig. 8.

The constitutive model using the neo-Hookean strain energy function was fit to the upper arm data with an error-of-fit of 34.8% (Fig. 10). The material parameters used to fit the model are displayed in Fig. 10.

6 Discussion

Skin forms the outermost layer of the human body and, because of its high visibility and importance, it has been studied in many areas of science and technology such as biomechanics, medicine, forensics, cosmetology and computer animation. In many of these applications, it is important to have accurate models of skin that capture its complex mechanical properties. Therefore, it is essential that

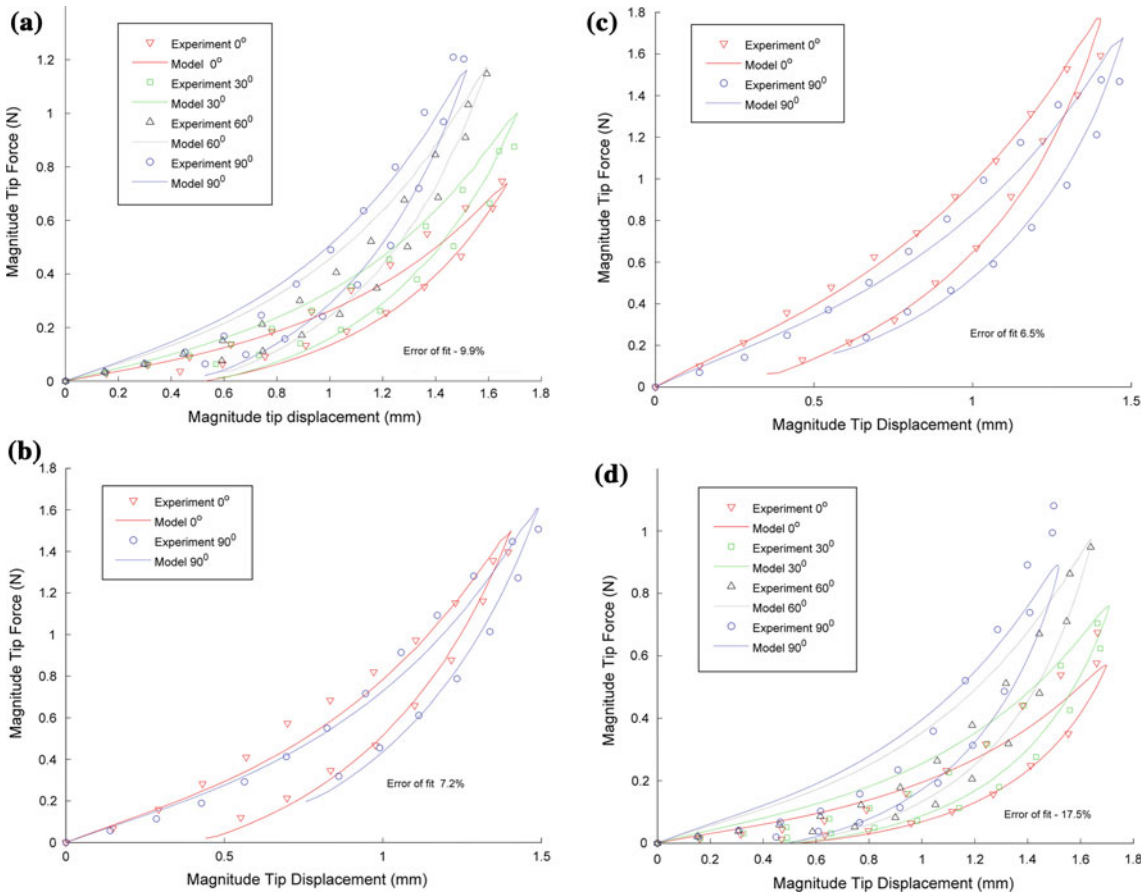

Fig. 7 Comparison of experimental and model force–displacement curves for in-plane deformation of skin on different parts of the *right arm*. The model parameters are in Table 1. **a** Posterior upper arm (*straight*); (**b**) Posterior upper arm (bent 90°); (**c**) Anterior upper forearm; (**d**) Anterior lower forearm

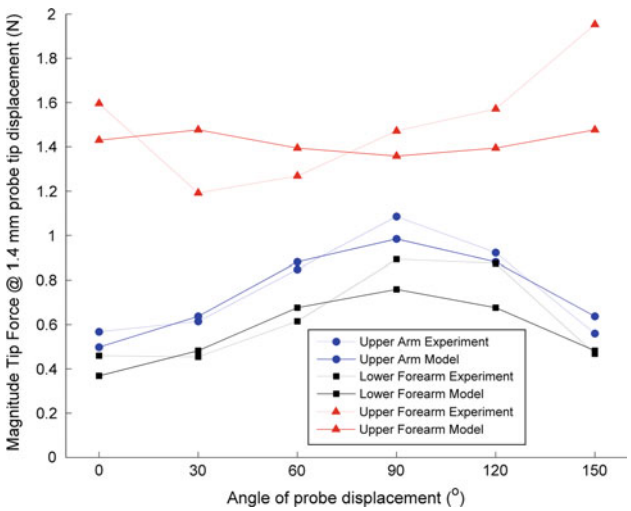

Fig. 8 Variation of the reaction force at 1.4 mm tip displacement with angle of tip displacement relative to the longitudinal axis of the arm

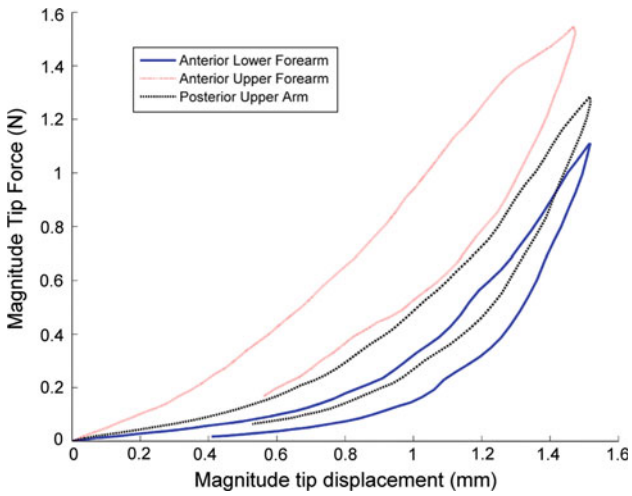

Fig. 9 Comparison of force response for the different skin areas. All data is for a probe displacement in a direction 90° to the longitudinal axis of the arm

experiments measuring the mechanical properties of skin be able to quantify its nonlinear, anisotropic and viscoelastic characteristics in vivo.

The experiments in this research measured the force response of different areas of in vivo skin when subject to in-plane deformations. For all areas of the arm tested, the

Table 1 Ogden, Prony series, and initial stress parameters used to fit finite element analyses to the average of the experimental data. The equivalent nominal pre-strain is also displayed

	μ (MPa)	α	$\bar{g}_1^P$	τ_1^G	σ_X(MPa)	σ_Y(MPa)	Equivalent strain		Error (%)
							ε_X	ε_Y	
Posterior upper arm (straight)	0.0096	35.993	0.3398	1.685	0.0011	0.0039	0.02	0.06	9.29
Posterior upper arm (bent)	0.0096	35.993	0.3398	1.685	0.0056	0.0051	0.07	0.06	7.23
Anterior upper forearm	0.0398	33.452	0.398	0.757	0.0076	0.0054	0.04	0.03	6.51
Anterior lower forearm	0.0026	35.883	0.459	0.828	0.0012	0.0041	0.06	0.1	17.5

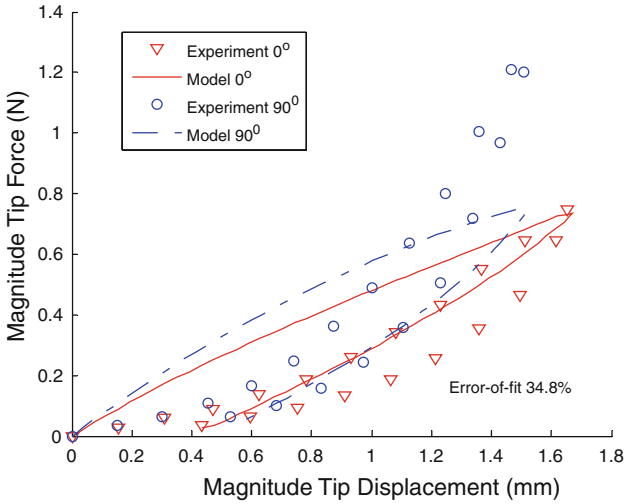

Fig. 10 Comparison of experimental and neo-Hookean model force–displacement curves for in-plane deformation of skin on the posterior upper arm. Model parameters: $C_1 = 0.02197$ MPa; $\bar{g}_1^P = 0.46496$; $\tau_1^G = 1.86102$; $\sigma_X = 0.00006$ MPa; $\sigma_Y = 0.05167$ MPa

skin behaviour was nonlinear and viscoelastic. The posterior upper arm and the anterior lower forearm also showed significant anisotropy. The experimental method in this research using a novel three-dimensional force-sensitive micro-robot is a significant improvement over previous experimental protocols such as suction, normal indentation, and torsion. With those protocols, the anisotropic characteristics of skin cannot be measured.

The experimental data were simulated accurately using finite element models with an Ogden strain energy function and quasi-linear viscoelasticity. The model captured the nonlinear force response of the skin in all areas. It also simulated accurately the hysteresis observed in the experiments, as well as any anisotropic characteristics. The errors-of-fit ranged from 6.5% for the anterior upper forearm to 17.5% for the anterior lower forearm (Table 1). When determining the material parameters in the nonlinear optimisation, the pre-stress in the X and Y directions were also used as model parameters. To the best of the authors' knowledge this approach has not been used when fitting models to in vivo experimental data on human skin. This allowed us to accurately fit an isotropic constitutive model to anisotropic experimental data.

It must be noted that the objective function in Eq. 6 will tend to weight the fitting towards the higher displacement region of the curves because the errors in this region are proportionally larger. An objective function that calculated the percentage error at each data point was investigated for one of the cases. This resulted in a better fit at lower displacements at the expense of a worse fit at higher displacements. The overall error-of-fit was greater than when objective function in Eq. 6 was used. The choice of objective function would depend on what region of the curve the study is interested in, i.e. in the low strain or high strain regions.

The Ogden material parameters determined in this study lie within the range of values reported in other studies. Evans and Holt (2009) report values in the region of $\mu = 130$ Pa and $\alpha = 26$ from studies on forearm skin (Note that their reported $\mu = 10$ Pa needs to be converted as a different form of the Ogden strain energy function was used.) Shergold and Fleck (2004) found $\mu = 0.1$ MPa and $\alpha = 9$ from in vitro tensile tests of lower abdomen skin. The values of μ and α varied significantly for the different parts of the arm tested in this study. It is probable that there would also be significant variations between individuals. The need to undertake a programme of testing many individuals and body regions as suggested by Evans and Holt (2009) is reiterated here.

The neo-Hookean strain energy function was unable to simulate the experimental data with the same accuracy as the Ogden model (Fig. 10). The model failed to capture the nonlinear response observed in the experiments and had an error-of-fit of 34% when simulating the deformation of the upper arm skin. This compares with an error-of-fit of 9.3% when the Ogden model is used to simulate the deformation of the same region. Therefore, the proposed model represents a significant improvement over previous in vivo models of skin. Models that characterise skin using a Young's modulus (Zahouani et al. 2009; Diridollou et al. 2000; Pailler-Mattei et al. 2008; Khatyr et al. 2006) or a neo-Hookean strain energy function (Delalleau et al. 2008) are unable to simulate accurately the experimental data in this research.

For the posterior upper arm area, the force response was measured when the arm was straight and when the arm was

Table 2 In vivo skin tensions reported in the literature

Study	Experiment type	Region	In vivo tension (N/m)	
			Longitudinal axis	Transversal axis
Diridollou et al. (2000)	Suction	Anterior forearm	12.35	–
Jacquet et al. (2008)	Extensiometry	Forearm	15	–
de Jong (1995)	Extensiometry	forearm	36	14
Present study	Multi-axial in-plane traction	Anterior lower forearm	1.8	6.15
Present study	Multi-axial in-plane traction	Anterior upper forearm	11.4	8.1
Present study	Multi-axial in-plane traction	Posterior upper arm (straight)	1.65	5.85
Present study	Multi-axial in-plane traction	Posterior upper arm (bent)	8.4	7.65

bent 90° (Fig. 7a, b). The model was able to fit the experimental data for both arm configurations with the same Ogden and viscoelastic material parameters. Only the pre-stress in the skin model was changed when the arm was bent. According to the model, the pre-stress in the direction of the longitudinal axis increased from 1.1 kPa when the arm was straight to 5.6 kPa when the arm was bent (Table 1). The pre-stress in the orthogonal direction increased slightly from 3.9 to 5.1 kPa. This result supports the hypothesis that it is only the tension in the skin that changes when a limb moves from one position to another. It also highlights the importance to note the orientation of the body when performing experiments to measure mechanical properties of skin in vivo.

The change in the corresponding pre-strain calculated in the model when bending the arm was 0.05 in the longitudinal direction and 0.0 in the transverse direction (Table 1). A rough estimation of the induced strain when bending the arm was made by measuring the change in dimensions of a rectangle drawn on the posterior upper arm. From this, the strain along the longitudinal axis of the arm when it was moved from a straight to a bent position was determined to be about 0.04. The corresponding strain in the transverse direction was 0.01. More accurate determinations of strain will be made in the future using digital image correlation techniques.

The proposed model has a significant advantage over other previous models in that it provides an estimate of the in vivo tension in skin. Many other in vivo models do not include in vivo tension as a parameter (Pailler-Mattei et al. 2008; Hendriks et al. 2006). There is a relative paucity of in vivo skin tension data in the literature. The in vivo tensions estimated in the present research can be compared with values found in the literature in Table 2. The in vivo tensions for the anterior upper forearm are slightly lower than the tensions measured by Diridollou et al. (2000) and Jacquet et al. (2008). The present study represents an improvement because an estimate of the in vivo tension in two orthogonal directions is provided. Diridollou et al. (2000) performed suction tests so could not estimate the in vivo tension in various directions due to the isotropic nature of the test. Qualitatively, the present results for the anterior upper forearm are comparable to the results of de Jong (1995). While de Jong (1995) estimates an in vivo tension higher than the present study, the in vivo tension in the direction of the longitudinal axis (36 Nm^{-1}) is greater than the in vivo tension in the transversal direction (14 Nm^{-1}), in agreement with the present study. The pre-strains that correspond to the pre-stresses ranged from 0.02 to 0.1 (Table 1). These are lower than the pre-strains of 0.2 reported by Evans and Holt (2009). As discussed earlier, further studies on a large number of individuals need to be undertaken to explain variations. The direction of the maximum in vivo tension measured at each point on the arm in this study approximately agreed with the accepted directions of the Langer or relaxed skin tension lines at those points (Fig. 11). The relaxed skin tension lines at the anterior lower forearm and posterior upper arm are aligned 90° to the longitudinal axis of the arm. On the anterior upper forearm, they are aligned approximately 30° to the longitudinal axis of the arm.

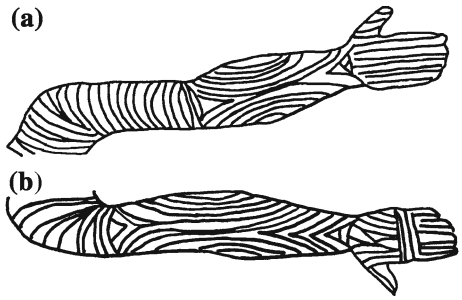

Fig. 11 Langer lines of the (**a**) posterior and (**b**) anterior areas of the right arm (Image adapted from MerckSource (2007))

The uniqueness of the identified model parameters in this study needs to be established. Ogden et al. (2004)

showed that it is possible to fit a model to experimental data accurately using multiple sets of model parameters. They found multiple 'optimum' sets of data when fitting models to simple tension and equibiaxial tension separately. For the optimisation procedure in this study, a richer set of experimental data was used. When determining the model parameters at each arm location, we fit the model to four data sets simultaneously (the probe was displaced in directions 0, 30, 60 and 90° relative to the longitudinal axis of the arm). Using multiple data sets simultaneously would improve the identification of model parameters. Ogden et al. (2004) also used Ogden strain energy functions with six and eight model parameters, whereas the Ogden strain energy function used in this study contained two model parameters. The uniqueness of model parameters is not limited to the Ogden strain energy function. It is also an issue with other models such as the Mooney–Rivlin function (Criscione 2003). Using as rich a set of experimental data as possible will increase the identifiability of the parameters of any material model.

There are several simplifying assumptions in the finite element model of skin in the present study. The skin is assumed to be a flat single homogeneous layer, whereas skin is a multi-layer material with each layer having a significant effect on the overall mechanical properties of the composite (Flynn and McCormack 2008a; Hendriks et al. 2006; Magnenat-Thalmann et al. 2002). In addition, the anchoring of the skin to the underlying structure has been ignored. This means that any shearing effects between the layers have been neglected. If a multi-layer model and mechanical anchorage were included, it is probable that the actual material stiffness of the skin in the model would be reduced, i.e. μ and α in the Ogden strain energy equation would decrease. Only the skin that lay within the boundary of the hole in the support plate was modelled. Soft tissue outside this area, the underlying layers, in particular, may have a significant effect on the force response. Material anisotropy, which is present in skin (Lanir and Fung 1974), has been ignored. The anisotropic response was modelled by applying an anisotropic pre-stress in the simulations. Incorporation of an anisotropic constitutive equation, such as one proposed by Lanir (1983), may improve the agreement between the experimental and model results. However, using a more complex anisotropic constitutive model presents additional challenges in relation to identifying unique material parameters and the in vivo tension field. A sufficiently rich set of experimental data will be needed to determine all the model parameters.

The model was fit to pre-conditioned experimental data. The viscoelastic model is too simple to simulate the pre-conditioning effect observed in the experiments. Future work will present a model that will simulate pre-conditioning accurately.

For the anterior lower forearm area, the model did not match the experimental data as well as the other skin areas (Error-of-fit 17.5%). Examining Fig. 9, the experimental force response for the anterior lower forearm is the most nonlinear of the three areas. The one-term Ogden model may not be sufficient to capture the high nonlinearity observed in the lower forearm area. A higher order Ogden or Arruda–Boyce strain energy function may simulate the experimental data in this area more accurately.

Future developments to the experimental method would include the ability to measure the strain field of the deformed surface of the skin. This can be achieved using three-dimensional digital image correlation methods. It is also planned to deform the skin using multiple probes. Both these developments will provide a very rich set of data, which can be used to accurately characterise the mechanical properties of skin in vivo.

Acknowledgments The authors would like to acknowledge the contribution of Albert Chen in the design and testing of earlier versions of the micro-robot. We wish to thank Peter Blythe for technical assistance in the design and production of the device.

Appendix: forward kinematics algorithm

The geometry of the problem is shown in Fig. 12. For given axes displacements, the tip of each axis (A, B, and C) is given by $\mathbf{p}_A$, $\mathbf{p}_B$, and $\mathbf{p}_C$. The length of the sides of the triangle ABC are

$$\begin{aligned} a &= |\mathbf{p_B} - \mathbf{p_C}| \\ b &= |\mathbf{p_C} - \mathbf{p_A}| \\ c &= |\mathbf{p_A} - \mathbf{p_B}| \end{aligned} \tag{8}$$

We can now find the lengths from each apex of the triangle ABC to the centroid of the moving platform $\mathbf{x}_{\text{cent}}$. From geometrical considerations and use of the cosine rule, the lengths x_A, x_B, and x_C are found by solving the following system of equations:

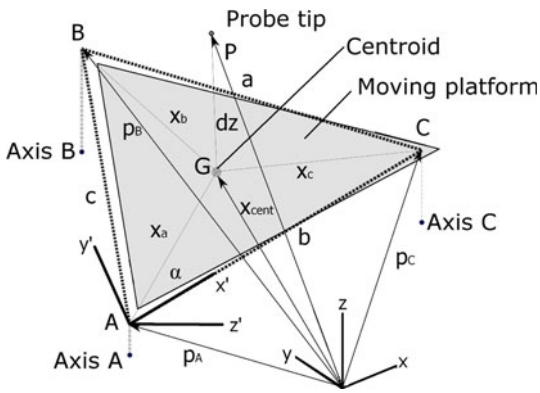

Fig. 12 Kinematic skeleton of the micro-robot

$$a^2 = x_B^2 + x_C^2 + x_B x_C$$
$$b^2 = x_A^2 + x_C^2 + x_A x_C \quad (9)$$
$$c^2 = x_A^2 + x_B^2 + x_A x_B$$

From the cosine rule, α, the angle between the lines AG and AC, is given by

$$\alpha = \cos^{-1}\left(\frac{x_a^2 - x_c^2 + b^2}{2x_a b}\right) \quad (10)$$

A local coordinate system is formed with the origin at A, the $x\prime$ axis along AC and the $z\prime$ axis normal to the moving platform. The centroid of the moving platform in the local coordinate system,$\mathbf{x}'_{\text{cent}}$, is then given by

$$\mathbf{x}'_{\mathbf{cent}} = \mathbf{p}'_{\mathbf{A}} + \begin{pmatrix} x_A \cos\alpha \\ x_A \sin\alpha \\ 0 \end{pmatrix} \quad (11)$$

The location of the probe tip in the local coordinate system is given by

$$\mathbf{P}' = \mathbf{x}'_{\mathbf{cent}} + \begin{pmatrix} 0 \\ 0 \\ dz \end{pmatrix} \quad (12)$$

$\mathbf{P}'$ is then transformed to the global coordinate system to give the location of the probe tip $\mathbf{P}$.

This algorithm was verified by comparing its results to the results of COSMOSMotion (Structural Research and Analysis Corporation, Concord, USA) simulations of solid models of the micro-robot.

References

Alexander H, Cook TH (1977) Accounting for natural tension in the mechanical testing of human skin. J Investig Dermatol 69:310–314

Batisse D, Bazin R, Baldeweck T, Querleux B, Lévêque J-L (2002) Influence of age on the wrinkling capacities of skin. Skin Res Technol 8:148–154

Bellamy K, Limbert G, Waters MG, Middleton J (2003) An elastomeric material for facial prostheses: synthesis, experimental and numerical testing aspects. Biomaterials 24:5061–5066

Bergstrom JS, Boyce MC (2001) Constitutive modeling of the time-dependent and cyclic loading of elastomers and application to soft biological tissues. Mech Mater 33:523–530

Bischoff JE (2006) Reduced parameter formulation for incorporating fiber level viscoelasticity into tissue level biomechanical models. Annl Biomed Eng 34:1164–1172

Bischoff JE, Arruda EM, Grosh K (2000) Finite element modeling of human skin using an isotropic, nonlinear elastic constitutive model. J Biomech 33:645–652

Cacou C, Muir IFK (1995) Effects of plane mechanical forces in wound healing in humans. J Roy Coll Surg Edin 40:38–41

Cavicchi A, Gambarotta L, Massabò R (2009) Computational modeling of reconstructive surgery: the effects of the natural tension on skin wrinkling. Finite Elements Analys Design 45:519–529

Cerda E (2005) Mechanics of scars. J Biomech 38:1598–1603

Criscione JC (2003) Rivlin's representation formula is Ill-conceived for the determination of response functions via biaxial testing. J Elastic 70:129–147

Daly CH (1982) Biomechanical properties of dermis. J Investig Dermatol 79:17s–20s

de Jong LAM (1995) Pre-tension and anisotropy in skin: modelling and experiments. Dissertation, Eindhoven University of Technology

Delalleau A, Josse G, Lagarde J-M, Zahouani H, Bergheau J-M (2006) Characterization of the mechanical properties of skin by inverse analysis combined with the indentation test. J Biomech 39:1603–1610

Delalleau A, Josse G, Lagarde JM, Zahouani H, Bergheau JM (2008) A nonlinear elastic behavior to identify the mechanical parameters of human skin in vivo. Skin Res Technol 14:152–164

Diridollou S, Patat F, Gens F, Vaillant L, Black D, Lagarde JM, Gall Y, Berson M (2000) In vivo model of the mechanical properties of the human skin under suction. Skin Res Technol 6:214–221

Evans SL (2009) On the implementation of a wrinkling, hyperelastic membrane model for skin and other materials. Comp Method Biomech Biomed Eng 12:319–332

Evans SL, Holt CA (2009) Measuring the mechanical properties of human skin in vivo using digital image correlation and finite element modelling. J Strain Analys Eng Design 44:337–345

Flynn C, McCormack BAO (2008a) Finite element modelling of forearm skin wrinkling. Skin Res Technol 14:261–269

Flynn C, McCormack BAO (2008b) A simplified model of scar contraction. J Biomech 41:1582–1589

Fung YC (1993) Biomechanics: mechanical properties of living tissues. Springer, New York

Gunner CW, Hutton WC, Burlin TE (1979) The mechanical properties of skin in vivo—a portable hand-held extensometer. Brit J Dermatol 100:161–163

Har-Shai Y, Bodner SR, Egozy-Golan D, Lindenbaum ES, Ben-Izhak O, Mitz V, Hirshowitz B (1996) Mechanical properties and microstructure of the superficial musculoaponeurotic system. Plast Reconstr Surg 98:59–70

Hendriks FM, Brokken D, Oomens CWJ, Bader DL, Baaijens FPT (2006) The relative contributions of different skin layers to the mechanical behavior of human skin in vivo using suction experiments. Med Eng Phys 28:259–266

Jacquet E, Josse G, Khatyr F, Garcin C (2008) A new experimental method for measuring skin's natural tension. Skin Res Technol 14:1–7

Khatyr F, Imberdis C, Varchon D, Lagarde J-M, Josse G (2006) Measurement of the mechanical properties of the skin using the suction test. Skin Res Technol 12:24–31

Kvistedal YA, Nielsen PMF (2009) Estimating material parameters of human skin in vivo. Biomech Model Mech 8:1–8

Lanir Y (1983) Constitutive equations for fibrous connective tissues. J Biomech 16:1–12

Lanir Y, Fung YC (1974) Two-dimensional mechanical properties of rabbit skin–II. Experimental results. J Biomech 7:171–174

Lott-Crumpler DA, Chaudhry HR (2001) Optimal patterns for suturing wounds of complex shapes to foster healing. J Biomech 34:51–58

Magnenat-Thalmann N, Kalra P, Leveque JL, Bazin R, Batisse D, Querleux B (2002) A computational skin model: fold and wrinkle formation. IEEE Trans Info Technol Biomed 6:317–323

MerckSource(2007) Langer lines. In: Dorlands Medical Dictionary. Elsevier. Available via http://mercksource.org/pp/us/cns/cns_hl_dorlands_split.jsp?pg=/ppdocs/us/common/dorlands/dorland/five/000060422.htm. Accessed 29 Oct 2009

Ogden RW, Saccomandi G, Sgura I (2004) Fitting hyperelastic models to experimental data. Computational Mechanics 34:484–502

Pailler-Mattei C, Bec S, Zahouani H (2008) In vivo measurements of the elastic mechanical properties of human skin by indentation tests. Med Eng Phys 30:599–606

Reihsner R, Balogh B, Menzel EJ (1995) Two-dimensional elastic properties of human skin in terms of an incremental model at the in vivo configuration. Med Eng Phys 17:304–313

Rubin MB, Bodner SR, Binur NS (1998) An elastic-viscoplastic model for excised facial tissues. J Biomech Eng 120:686–689

Schneider D (1982) Viscoelasticity and tearing strength of the human skin. Dissertation, University of California

Shergold OA, Fleck NA (2004) Mechanisms of deep penetration of soft solids, with application to the injection and wounding of skin. Proceedings of the Royal Society A: Mathematical. Phys Eng Sci 460:3037–3058

Shoemaker PA, Schneider D, Lee MC, Fung YC (1986) A constitutive model for two-dimensional soft tissues and its application to experimental data. J Biomech 19:695–702

Silver FH, Freeman JW, DeVore D (2001) Viscoelastic properties of human skin and processed dermis. Skin Res Technol 7:18–23

Wan Abas WAB (1994) Biaxial tension test of human skin in vivo. Bio-Med Mater Eng 4:473–486

Wilkes GL, Brown IA, Wildnauer RH (1973) The biomechanical properties of skin. Crc Cr Rev Biom Eng 1:453–495

Zahouani H, Pailler-Mattei C, Sohm B, Vargiolu R, Cenizo V, Debret R (2009) Characterization of the mechanical properties of a dermal equivalent compared with human skin in vivo by indentation and static friction tests. Skin Res Technol 15:68–76